A Pneumatic-Actuated Feel-Through Wearable Haptic Display for Multi-Cue Delivery

Giulia Pagnanelli, *Graduate Student Member, IEEE*, Giovanni Latella, Manuel G. Catalano, *Member, IEEE*, and Matteo Bianchi, *Member, IEEE*

***Abstract*—Compared to the "Seeing-through" paradigm for the concurrent display of both real and virtual images in vision-enabled Augmented Reality (AR), its haptic counterpart, i.e., the "Feeling-through" via wearable tactile systems, which enables to experience simultaneously physical objects and haptically rendered virtual properties, is still largely unexplored. In a previous work, we introduced the Wearable-Fabric Yielding Display (W-FYD), which uses an elastic thin fabric as the interaction surface with the finger, allowing the delivery of softness-related cues both in active and passive exploration mode, together with sliding stimuli. The device was proven effective, but the current design faces form factor issues related to the dimensions and weight of the device, due to the actuation strategy of the lifting mechanism in the passive mode. To tackle this issue, we propose a miniaturized version of the system, named the W-FYD AIR, which allows reducing the overall dimensions of the device, from 100 × 60 × 36 mm to 78 × 45 × 37 mm, and its weight, from 100 g to 54 g, by exploiting pneumatically-actuated chambers for the lifting mechanism. Through careful sizing of each component and a process of characterization and identification, we demonstrated that the new system attained the same characteristics and functionality as the original one.**

***Index Terms*—Haptics and haptic interfaces, mechanism design, wearable robotics.**

Received 19 July 2024; accepted 28 November 2024. Date of publication 18 December 2024; date of current version 26 December 2024. This article was recommended for publication by Associate Editor H. Kajimoto and Editor J.-H. Ryu upon evaluation of the reviewers' comments. This work was supported in part by the Italian Ministry of University and Research (MUR) - Fondo Italiano per la Scienza (FIS), under PERCEIVING Grant FIS00001153, in part by the Italian Ministry of Education and Research (MUR) in the framework of the ForeLab Project (Departments of Excellence), in part by the European Union by the Next Generation EU Project ECS00000017 'Ecosistema dell' Tuscany Health Ecosystem (THE, PNRR, Spoke 9: Robotics and Automation for Health), in part by the Project 'EXPERIENCE' through European Commission H2020 Framework Programme under Grant 101017727, and in part by the Università di Pisa through the 'PRA Progetti di Ricerca di Ateneo' (Institutional Research Grants) under Project PRA 2022 27 'ART'. *(Corresponding author: Giulia Pagnanelli.)*

This work involved human subjects or animals in its research. Approval of all ethical and experimental procedures and protocols was granted by the Bioethical Committee of the University of Pisa under Application No. 30/2020.

Giulia Pagnanelli and Matteo Bianchi are with the Centro di Ricerca "Enrico Piaggio", Universita' di Pisa, 56122 Pisa, Italy, and also with the Dipartimento di Ingegneria dell'Informazione, Universita' di Pisa, 56122 Pisa, Italy (e-mail: giulia.pagnanelli17@gmail.com).

Giovanni Latella is with the Dipartimento di Ingegneria dell'Informazione, Universita' di Pisa, 56122 Pisa, Italy.

Manuel G. Catalano is with the Centro di Ricerca "Enrico Piaggio", Universita' di Pisa, 56122 Pisa, Italy, and also with the Soft Robotics for Human Cooperation and Rehabilitation, Istituto Italiano di Tecnologia, 16163 Genova, Italy.

This letter has supplementary downloadable material available at https://doi.org/10.1109/LRA.2024.3519894, provided by the authors.

Digital Object Identifier 10.1109/LRA.2024.3519894

I. Introduction

In recent decades, the rapid advancement of technology has given rise to a new generation of haptic systems designed to enhance human experience and interaction with the environment, i.e., Wearable Haptic Systems (WHS). These devices aim to artificially reproduce the sense of touch by providing users with skin-mediated feedback through mechanical stimuli such as vibrations, pressure, and other tactile cues; see [1] for a review on this topic. WHS has found a fertile field in many robotic and advanced human-machine interaction (HMI) areas, such as assistive technologies [2], [3], virtual reality [4], [5], and telemanipulation via remote robotic systems [6], [7], among the others. WHS has the advantage of being able to be comfortably worn by the user, who can experience a more natural HMI, without (or minimally) affecting the natural execution of the interactive task. The literature presents haptic devices designed to be worn on the arms, feet, and wrists, although the majority focuses primarily on the finger [1].

Most WHS exploits rigid surfaces to deliver mechanical stimuli and interact with the skin, which can affect the user's cutaneous response during real object exploration, masking touch-evoked perception. This makes them unsuitable for tactile Augmented Reality (tAR) as "*Feel-through* wearables, which should allow the perceptual response yet maintain the capability of modifying the tactile representation of the explored objects, via the delivery of artificially rendered tactile stimuli [8]. Functional materials like dielectric elastomer actuators (DEAs) have recently been used to create *Feel-through* WHS [8], [9], mainly for vibrotactile feedback. Other methods use electro-tactile stimulation integrated into temporary tattoos to deliver vibration stimuli [10]. In [11], an electrotactile film with reduced-size holes enables direct contact with external objects, while [12] introduced a nail-mounted foldable haptic device to render touch-related contacts via the vibration using a linear resonant actuator for mixed reality. Although promising, these approaches were not designed to modulate softness perception. Looking at this aspect, only a few wearables were proposed for tactile augmented reality. In [13], authors increase the perceived compliance of a real object by controlling pressure at the middle phalanx. However, the system allows only a binary perception alteration and cannot be considered *Feel-through*. In [14], a rigid ring reduced finger-pad deformation by pressing on it while allowing direct skin contact with the environment at the fingerpad center. Nevertheless, this device works only for items smaller than the fingerpad and enables only a simple switch on the perceived softness state. To conclude, in the State of the Art, no solutions offer *Feel-through* softness perception with modulation of the user's perception in tactile augmented reality. To bridge this

© 2024 The Authors. This work is licensed under a Creative Commons Attribution-NonCommercial-NoDerivatives 4.0 License. For more information, see https://creativecommons.org/licenses/by-nc-nd/4.0/

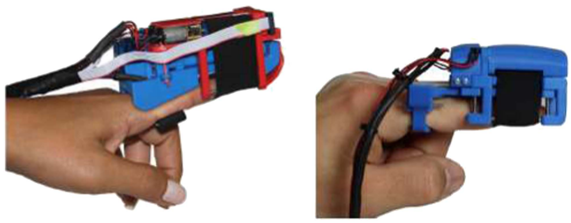

(a) (b)

Fig. 1. W-FYD devices. (a) Shows the W-FYD with $100 \times 60 \times 36$ mm for 100 g while (b) the new miniaturized version, W-FYD AIR, with $78 \times 45 \times 37$ mm for 54 g.

gap, in [15], we proposed a fabric-based WHS for the finger, the W-FYD [16]. W-FYD uses a thin elastic fabric (less than 1 mm) attached to two DC motors and a lifting mechanism driven by a servomotor. The lifting mechanism warps the fabric around the user's finger, and the DC motors maintain the fabric in a resting stretching state, avoiding any perceivable force. Based on the force exerted by the user on the deformable object, the lifting height is varied to simulate different contact area growths. Various perceptions of softness can be achieved by controlling the expansion of the contact area, making objects feel softer as the lifting mechanism enables larger vertical displacements. This strategy ultimately determines the contact area spread rate w.r.t. the indenting force [17], which was proven to be a key element in the human cutaneous perception of softness. We also demonstrated that the fabric does not affect the natural cutaneous perception of the external items.

The W-FYD was designed to enable both active and passive softness exploration and is also able to induce a sliding effect under the finger pad. In the passive mode, a servo motor controls a lifting mechanism composed of two camshafts connected by gears that bring the fabric in contact with the finger pad conveying a tactile cue on the skin. The stretching condition of the fabric can be modulated to reproduce the required stiffness profile by controlling the positions of two DC motors attached to the fabric. The device was successfully integrated into robotics-enabled tele-palpation tasks for gynecologic surgery, delivering compliance information on uterine tissues [7], and in tAR training to simulate artery pulses with inert artificial biological organs. Despite its effectiveness in providing tactile cues, participants in our previous work [7] reported that the device's dimension and weight needed improvement to enhance the overall wearability, form factor, and comfort. To tackle this issue, we analyzed the components contributing most to the system's size and weight. While reducing the footprint of the DC motors could help, including the possibility of using flexible drive shafts, they are not the main factor considering DC dimensions ($l = 49.25$ mm, $d = 5.50$ mm comprised the cylinder to fix the fabric tissue and the magnet for the encoder). Therefore, we focused on the lifting mechanism's actuation in passive mode (i.e. a servomotor, dimensions ($23.88 \times 11.30 \times 32.81$ mm, and a camshaft mechanism, dimensions $70.22 \times 22.00 \times 22.00$ mm). We propose a miniaturized version of the system, hereinafter referred to as W-FYD AIR (Fig. 1), which allows to reduce the overall dimensions of the device from $100 \times 60 \times 36$ mm to $78 \times 45 \times 37$ mm and its weight from 100 g to 54 g, by exploiting pneumatically-actuated chambers for the lifting mechanism. It is worth noticing that our effort focused on the miniaturization of the device itself. In the next section, we also discuss the implications of our choices for the off-the-device components. The work involved several steps: we started by revising the design to miniaturize the structure and integrate the new pneumatic actuation system. For the pneumatic actuation mechanism, we opted for a silicone chamber that inflates and deflates, enabling the frame to move vertically. Next, we developed a control architecture for both the pneumatic actuator and the DC motors that move the fabric. To opportunely define and test the functioning of our device, we evaluated its force-indentation and pressure-displacement characteristics and identified the system's transfer function (TF) between the motor pump input and the output displacement of the lifting mechanism. While demonstrating that the re-designed W-FYD AIR retained the same stiffness workspace, TF, and dynamic response as the previous version, we also test the effectiveness of W-FYD AIR by performing experiments with 5 human participants. Results showed that W-FYD AIR reliably delivered different softness levels in both active and passive modes and provided a clear perception of sliding. This indicates that the miniaturized version, retains all the functionality of the original one, with improved wearability due to its reduced size and weight.

II. W-FYD

The W-FYD presented in [16] is a wearable haptic interface for the finger that delivers controllable softness-related cues. The base is fixed and contains a lifting mechanism. The frame hosts the two DC motors (Pololu 298:1 Micro Metal Gearmotor), which independently actuate two rollers attached to the elastic fabric (Superbiflex HN by Mectex S.P.A), whose stretching state is controlled by varying the motor angles θ_1 and θ_2, with θ_1 = - θ_2 (assuming positive counterclockwise rotations). Two pins connected to the frame allow fingertip interaction with the fabric while it is pulled. The W-FYD operates in three modes: *active*, where the user actively flexes the distal phalanx to probe the fabric surface; *passive*, where the finger is still, and the lifting mechanism presses the fabric against the fingerpad; and *sliding*, where synchronized motor movement slides the fabric against the fingerpad. A unique feature of W-FYD is its ability to decouple stiffness rendering from force delivery, as fabric stretching and lifting are actuated separately in passive mode. The device can reproduce non-linear stiffness characteristics within its stiffness workspace by knowing the indentation value δ and using a power function $F(\delta) = \lambda\delta^{\beta}$ which describes the stiffness behavior, where β is an exponent and λ is determined by motor position. Considering

$$\lambda = \frac{F}{\delta^{\beta}} = \frac{\sigma(\theta)\delta}{\delta^{\beta}} = \frac{a e^{b\theta}}{\delta^{\beta-1}}, \qquad (1)$$

the motor position can be calculated as $\theta = \log(\frac{\lambda\delta^{\beta-1}}{a e^{b}})$, based on the fabric's stretch. Note that, in active mode, δ is measured by a contact-less infrared (IR) sensor (Avago HSDL-9100), and in passive mode, it corresponds to the height variation of the moving frame enabled by the lifting mechanism. This mechanism is actuated by a servomotor (HS-5055MG Servo by Hitec) and consists of two camshafts connected by gears. The height is given by $h_p = h_0 + L \sin\alpha$, where L is the shaft arm length, α is the angle between the shaft arm and horizontal plane, and h_0 is the shaft radius. For further details, please refer to [16].

III. W-FYD AIR: System Description

The W-FYD AIR (Fig. 1) is the miniaturized evolution of the W-FYD proposed in [16], featuring significant reductions in dimensions and weight that enhance comfort and wearability.

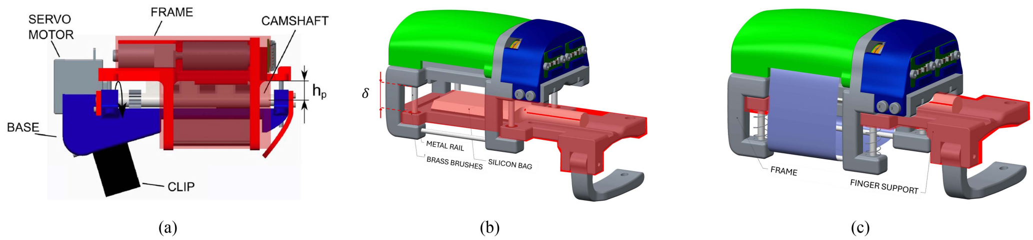

Fig. 2. Comparison between the lifting mechanism actuation in passive mode for W-FYD (a) and W-FYD AIR (b), (c). (b) shows the bag deflated, with the frame in its static condition, while (c) shows the bag inflated, causing the frame to move. All moving components are highlighted in red.

Specifically, the new device measures $78 \times 45 \times 37$ mm and weighs 54 g, compared to $100 \times 60 \times 36$ mm and 100 g for the previous W-FYD. The overall architecture remains similar, as do the three interaction modes (active, passive, and sliding). The key improvement in this new version, which allows for reducing the overall dimensions, lies in the actuation of the lifting mechanism, which now utilizes pneumatic actuation instead of the previous servo motor-camshaft solution. This involves embedding a soft bag between the base and the moving frame, with air supplied by a pump motor placed outside the device, connected via a small tube. When the bag inflates, it lifts the frame, allowing it to slide while pressing the fabric against the finger (Fig. 2(b) and 2(c)). Fig. 2 illustrates the different passive actuation mechanisms of the new version compared to the old one.

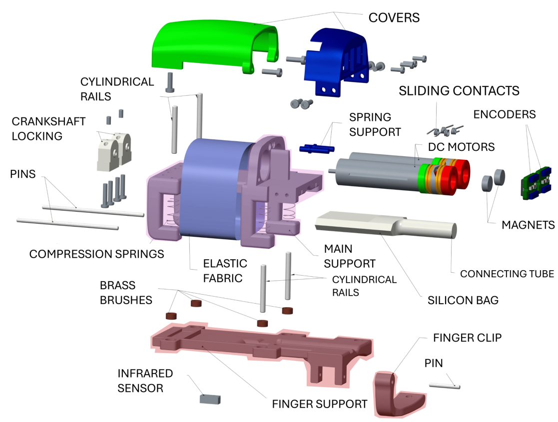

Fig. 3. W-FYD AIR exploded view. Main and moving frames are highlighted in pink and red, respectively.

A. Structure Design and Components

Hosting the new actuation involved redesigning the overall structure. More specifically:

- *Main support:* The main support (frame) was opportunely modified to make it compatible with the new moving support. We designed a hollow on the surface for placing the silicone bag and the connection tube. We positioned on each of the four cylindrical rails - which connect the main and the moving frames - a compression springs (Vanel C.030.018.0120.I). We iteratively tested different springs in the range 0030.I - 0260.I, to find the best solution that ensures adequate dynamic response of the overall system (see Section IV-C), enabling the moving frame to elastically return to the initial static condition, without affecting the lifting mechanism. Two torsional springs were also fixed to the frame to get in contact with the motors ensuring stable contact. Similarly to the W-FYD, the frame hosts two DC motors, with a reduced footprint, Maxon DCX6 with a planetary gearbox GPX6 (dimensions $l = 40.15$ mm, $d = 5.00$ mm), mounted with their shafts locked to the frontal camshaft locking (see Fig. 3, allowing the rollers (cylinder that cover the motor and host the fabric) to rotate around the longitudinal axis when activated. An integrated planetary gear system provides high torque output, which is important to avoid larger DC motors, contributing to the system miniaturization. Each motor is also equipped with a small magnet that enables reading motor angular position through encoders with 12-bit resolution (Auster Microsystem AS5045).
- *Moving Frame:* The four lateral supports of the moving frame have been oriented in the longitudinal direction to guarantee a larger space for hosting the finger (Fig. 3 highlighted in red). We designed a hollow to host the silicone bag and the connection tube and the frame length to have a comfortable clip, which hosts the proximal phalanx and maintains the user's finger between the frame and the fabric, preventing rotation (Fig. 3 highlighted in pink). This ensures wearability and correct finger alignment. The moving frame is also equipped with a contactless infrared (IR) sensor (Avago HSDL-9100), with a range of 0 to 60 mm used to measure indentation variations made by the finger movements in the active mode. Finally, as for the W-FYD, the frame features two pins around which the elastic fabric is wrapped, keeping its surface always extended.
- *Others:* The rear cover (blu in Fig. 3) attached to the moving frame was dimensioned to maintain stable contact with the motors. This also ensures that the sliding contacts in the correct position, aligning the encoders (fixed to the cover using two screws each) with the motor magnet, and making the structure stable. The new cover also guarantees not increasing the lateral dimension of the whole device. Frontal cover (green in Fig. 3) was redesigned to cover the new main support.
- *Remotized Componets:* The motor pump, the electro-valve, and the pressure sensor are remotized in a dedicated case such as the electronic boards (Fig. 4). Specifically, we used two custom-made electronic boards (PSoC-based with RS485 communication protocol) to control the system: one manages motor positions based on encoder readings and acquires IR sensor measurements, and the other controls the inflating system. The idea is to incorporate all these components into a compact case that can be worn on the forearm, thus not affecting the length of the silicone tube needed for inflating the chamber and increasing the freedom of movement.

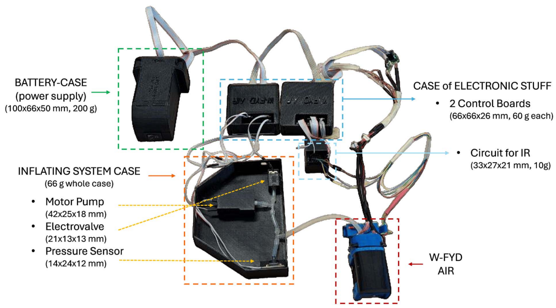

Fig. 4. System Components.

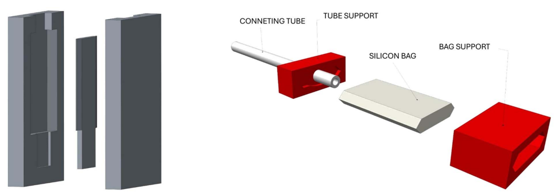

(a) Silicone casting in a mold (b) Casting system with tube.

Fig. 5. Silicon bag realization.

Fig. 3 provides an overview of the W-FYD AIR CAD model, showcasing all structural parts made from ABSplus—Stratasys rapid prototyping material. Additionally, Fig. 4 displays a view of all the components.

B. Inflating System

The pneumatic actuation system consists of four main components: an inflatable soft bag, a pump motor, an electrovalve, and a pressure sensor. The inflatable bag plays a fundamental role in the development of the new actuation system. It must be made of resistant soft material, with a preferential inflating direction, and it has to be able to inflate almost 1cm, occupying minimal space in the rest condition. Testing several solutions, the use of silicone bags has proven to be the best. Specifically, we produced the bag by casting the silicone Smooth on Dragon Skin 10 FAST in a mold with a plastic core. The whole realization procedure consists of four main steps: i) assembling the external mold and the core and casting the silicone; ii) removing the plastic core from the obtained air chamber through the open side; casting other silicon in the cavity on the support surface through a rubber tube inserted in the bag cavity in order to stick the open side of the silicone bag to the surface and close it; iv) after the cure time, glut the tube with a silicone glue (Smooth on Sil-Poxy) to the resulted silicone bag (Fig. 5). It is worth noting that the inflation and deflation times impact the system response. Taking this into account, we appropriately sized the silicon chamber and the tube connecting it to the motor pump, testing different dimensions, to ensure a system response comparable to that of the previous device, i.e., suitable for staying within the desired operating range for the proper delivery of tactile stimuli. Specifically, we evaluate the step response of the inflating system, in terms of the rise time, with a pressure reference of 200 mmHg. Results obtained for the chosen dimensioning (bag: $30.0 \times 15.75 \times 0.75$ mm, tube: $l = [10 - 15]$ mm, $d = 3$ mm) indicate that the system achieved 90% of the reference pressure in approximately 0.27 s, 95% in 0.41 s, and 99% in 0.6 s, demonstrating a timely response comparable to [16]. To achieve this, as pump motor and electrovalve, we chose the Conjoin CJP31-C03A1 DC 3V, and Conjoin CJV10-C03A1 DC 3V, respectively. The pump is actuated by a motor thus the inflating air flow can be modulated by controlling the supply voltage. The valve consists of a solenoid that, if activated, attracts an iron mass, blocking the airflow. We took the Phidgets as an absolute pressure sensor and characterized it in the range of [0, 840] mmHg by utilizing a compressor and the pressure regulator system Electro-pneumatic Regulator ITV1000/2000/3000. Then, we found the relation between the sensor output voltage and the real pressure through a fitting procedure. With a goodness of fit R^2 of 0.99, it resulted equal to $P = 1.9V - 699$, where P is the relative pressure in mmHg and V is the voltage in mV.

C. Control Architecture

Controlling the W-FYD AIR means designing suitable control strategies for both fabric stretching and inflating systems according to the work modality (active, passive, or sliding). We developed two separate control loops: the first one concerning the two DC motors and the encoders aimed to control the fabric stretching and sliding condition - related to both the active and passive mode as well as with the sliding cue delivery - and the second one finalized to manage the inflating system for the passive exploration mode.

1) DC Motors System Control: We implemented a position-current double control loop; the position controller generates the reference current, while the current controller produces the PWM output to the motor, preventing excessive overheating. Motor angles are set as $\theta = -\theta_1 = \theta_2$ for fabric stretching: positive θ stretches the fabric, and negative θ relaxes it. Fabric sliding modulation is performed by setting $\theta = \theta_1 = \theta_2$. We tested the motors' response to positive θ steps of 45° and 90°, yielding rise times (from 10% to 90%) of 0.11 s and 0.17 s, with steady-state tracking errors of 0.9% and 0.5% respectively. The motors' response were also tested involving a sinusoidal reference at frequencies of 1 Hz, 2 Hz, 5 Hz, and 10 Hz with an amplitude of $\theta = 45^\circ$. Below 5 Hz, the motor accurately follows the reference position, while significant delays occur beyond 7 Hz.

2) Inflating System Control: The control strategy features two states: the valve is closed and the pump activated, the bag inflates; the valve is open, and the bag deflates. The pressure sensor enables closed-loop pressure regulation within the pump operational range (0–350 mmHg), comparing the desired (reference) pressure with the measured pressure and using the difference (error) to manage the inflating system. We modulate the pump supply voltage through a PWM signal to control airflow. The inflating system dynamics depends on the operating point: higher reference pressures require increased activation voltage for the pump airflow, hence higher pump supply voltage. Therefore, we designed a proportional controller with saturation. However, even if it regulated the bag pressure effectively, it caused oscillations in valve operation, leading to not negligible noise and potential valve damage. To mitigate this, we developed a control strategy that considers the bag state (inflating or deflating) at previous step. Basically, the valve is kept closed when the reference pressure is constant or increasing and is opened only when the reference decreases, provided the bag pressure is above the new reference. Overshoot during inflation will not trigger bag deflation to maintain stability and avoid oscillations. Therefore, having information about the state allows for defining the desired valve state. On the other hand, the bag pressure regulation in different fabric stretching states induced by the DC motors

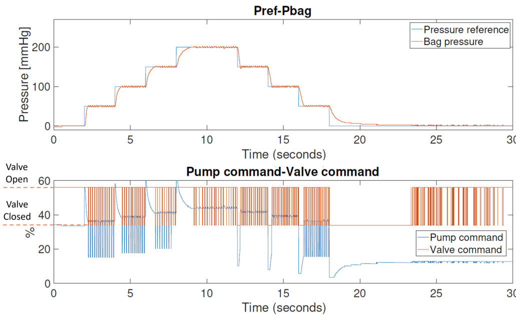

(a) Result of Control Strategy not considering bag state

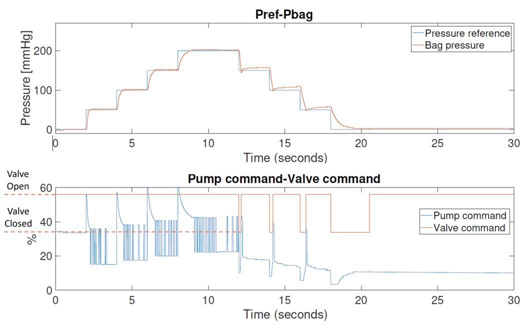

(b) Result of Control Strategy considering bag state

Fig. 6. Result of Control Strategy not considering bag state (a) and considering bag state (b). Plots on top show the system step response with reference pressure in blue and the measured pressure in red; plots on the bottom report the percentage of voltage V_{dc} for the air pump in blue and the valve state in red (low = open, high = closed).

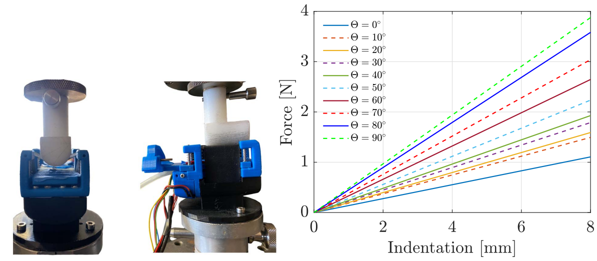

(a) Frontal (b) Lateral (c) Force-Indentation characteristic.

Fig. 7. Force-Indentation characterization. (a) and (b) show two different views of the used setup, focusing on the white head indenting the fabric. (c) show the plot of the Force-Indentation characteristic in N/mm.

constitutes the basis for moving the frame in passive mode. A higher pressure is required for stiffer fabric. Hence, open-loop position control based on a Look-up table is not recommended and a position measure of the moving frame is needed for a suitable closed-loop control. Accordingly, we implemented a two-loop control system. The outer loop modulates the reference pressure based on the frame position error, while the inner loop regulates the bag pressure as described. This approach ensures that the inflating system regulates the bag pressure to reach the desired moving frame position. Note that, a frame control solely based on position information would be ineffective, since the required pump supply voltage for airflow varies with pressure. Finally, while fabric stiffness affects pressure dynamics, tests show that our controller effectively regulates bag pressure across varying fabric stiffness values.

Tests were conducted with the device worn on the user's finger. The fabric is initially set to the no pre-stretched state, and then the pressure is controlled by steps of 50 mmHg amplitude, from 0 to 200 mmHg, activating the lifting mechanism, and then back to 0. As previously discussed, the control law varies depending on the reference pressure and allows the system to follow the reference up to 200 mmHg. When the reference pressure decreases, the valve opens for bag deflation. In Fig. 6 we reported results obtained with and without incorporating bag state information in the controller. The chosen controller effectively eliminates valve oscillations (Fig. 6(b)), which are evident in Fig. 6(a). The proposed control strategy shows improved performance in following pressure references, although the time delay from the valve command to its actual closure causes some negative overshoot. The test was also conducted considering two fabric stretching states, i.e., $\theta = 45^\circ$ and $\theta = 90^\circ$, with comparable results.

IV. System Characterization

In this section, the characterization of the W-FYD AIR in terms of force-displacement and pressure-displacement is discussed to define the stiffness workspace reproducible in both active and passive modalities. The control strategies for both work modalities were reported, with a focus on the passive mode utilizing the new pneumatic actuation. We also outline the identification process adopted to determine the W-FYD AIR transfer function between control inputs of the motor pump, i.e., the pressure and measured output displacements of the lifting mechanism in the passive condition.

A. *Force-Indentation Characterization*

As the first step towards the definition of the W-FYD AIR control, we characterized its workspace, in terms of force F in N and indentation δ in mm. A procedure similar to the one in [16] was adopted, utilizing the Instron Zwick/Roell Z005 Table Top materials testing machine, which allows for performing a controlled indentation (with an accuracy of 1 μm) on the fabric along the vertical axis and collecting corresponding force data (with an accuracy of 1 mmN). Various fabric stretching states were considered by changing the angular position of both DC motors θ_1 and $\theta2$, such that $\theta = -\theta_1 = \theta_2$, ranging from 0 to 90 degrees with 10 degrees of incremental step. Then, the state stretching condition was described by the couple (θ_1, θ_2). A custom support was designed using CREO 5 and 3D-printed in ABS to position the device under the machine. A CNC-machined indenter head was created with radius $r = 7.5$ mm and length $L = 30$ mm, modeling the human fingertip as in [16], to induce the controllable vertical displacement. Figs. 7(a) and 7(b) report the overall setup. We tested each stretch condition by probing the fabric with the indenter, considering a single indentation step of 8 mm and a fixed velocity equal to 0.5 mm/s. An emergency stop was triggered for forces exceeding 10N to avoid damage the device. The force-indentation data recorded in a *.csv* file were opportunely filtered and fitted with a linear interpolation over the stretch conditions. The obtained curves, with a goodness of fit $R^2 > 0.97$, are reported in Fig. 7(c). Thus, the force-indentation characteristics can be written as a function of θ as $F = \sigma(\theta)\delta$, where F is the indenting force, δ is the indentation and $\sigma(\theta)$ is the function that provides the stiffness coefficient for a given value of θ equal to

$$\sigma(\theta) = ae^{b\theta} = 0.1485e^{0.01334\theta}, \quad (2)$$

with a goodness of fit $R^2 = 0.9906$.

This demonstrates that the W-FYD AIR can reproduce linear stiffness relying on the reported characterization. Considering

(2), motor position θ, associated with a given linear stiffness coefficient, can be evaluated as $\theta = log(\frac{\sigma}{ae^b})$.

Any arbitrary non-linear stiffness characteristic can also be reproduced within the device stiffness workspace, as with the previous version. The motor position control can be determined using (1), considering that, in the passive mode, δ is determined through the pump motor's commanded pressure that induces the desired displacement of the mobile frame. It is worth noting that for a given value of λ and β for reproducing the desired stiffness profile, and for a given indentation δ, the required value of θ are coherent with those obtained for the W-FYD in [16]. Therefore, we demonstrate that the new W-FYD AIR covers the same stiffness workspace as W-FYD, ranging from 0.17 to 0.48 N/mm.

B. Pressure-Displacement Characterization

The second step towards the definition of the W-FYD AIR control involved the characterization in terms of pressure P in mmHg and displacement δ in mm. This step allows establish the relation between the bag inflation and the resulting displacement of the moving frame.

A passive marker-based motion tracking system (OptiTrack - Motion Capture Systems) was used to measure the effective displacement of the lifting mechanism due to bag inflation. Unlike in [16] where two markers were placed, we used five markers, one in the frontal face of the device and two pairs on the right and left sides. This configuration allowed us to assess whether the inflated bag caused any asymmetric displacement of the moving frame. A device's support to stabilize the device during data collection and a plastic human finger were designed with CREO 5 parametric and 3D-printed.

For data collection, we developed a Matlab/Simulink scheme to control the inflating system and exploited the Vision Motive Tracker 2.2 software to acquire MoCap data. After setting the fabric in its initial, no pre-stretched, configuration, we controlled the bag pressure by steps of 50 mmHg amplitude, from 0 to 200 mmHg, holding each reference for 4 seconds. For each pressure step, we performed ten repetitions and saved the pressure in a *.mat* file with a sample rate of 200 Hz and the MoCap measurements in a *.csv* file at 120 Hz. Due to the different sampling rates of the two measurement systems, we re-sampled the pressure data to have the data series at the same frequency, checking for possible loss of information. We fitted data of each couple of data series independently, finding that the best equation to approximate the pressure-indentation behavior is linear. Tested the coherence between the relations, we considered the mean of the ten obtained, within the pressure range [0–200] mmHg, as the pressure-indentation relation of our system:

$$P(\delta) = 60.06\delta - 34.69, \quad \text{or similar} \quad \delta(P) = \frac{P + 34.69}{60.06}. \tag{3}$$

With the new pneumatic system, W-FYD AIR in passive mode can vary δ ranging from 0 to 3.9 mm if we remain in the cautionary limits (in terms of bag inflating) of $P = 200$ mmHg and from 0 to 5.5 mm if we reach 300 mmHg. This agrees with the h_p's range obtained with the W-FYD.

C. System Identification

The same setup presented in Section IV-B was also used to gather data for the system identification process, aimed at retrieving the transfer function between the commanded input to the pump motor and the effective indentation generated by the device. Indeed knowing the TF allows evaluating system's bandwidth for passive touch interaction. In this experimental phase, we used chirp signals as pressure input signals and recorded the corresponding displacements of the mobile frame as output signals. Three different magnitudes were used for the chirp signals, i.e., 100 mmHg, 150 mmHg, and 200 mmHg, each lasting 30 seconds. Input and output signals were resampled at 120 Hz. resulting in an amount of 3600 samples, split into 3000 for identification and 600 samples for cross-validation. In order to find the best model in terms of a good balance between complexity and adequacy criterion results, we tested several polynomial models of ARX, OE, and ARMAX. The ARX model, with parameters $n_a = 1$, $n_b = 1$, $n_k = 1$, provided the best trade-off between goodness and complexity achieving a Fit to estimation data (FtED) of 95.66% (compared with obtained FtED for ARMAX models less than 92% and for OE model less than 84%) and a Final Prediction Error (FPE) of 2.8014e-04.

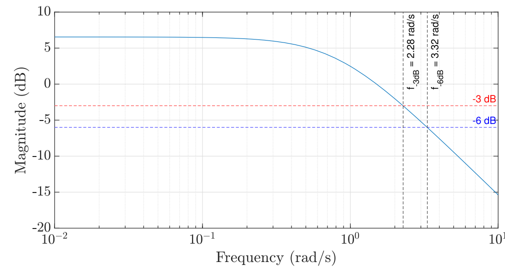

Fig. 8. Bode diagram of the ARX Model; red and blue lines representing the −3 dB and the −6 dB bandwidth, respectively.

TABLE I
CONFUSION MATRIX FOR RELATIVE RECOGNITION TASK: ACTIVE AND PASSIVE MODE

ACTIVE	SH1	SH2	SH3	Relative Accuracy
SH1	28	0	1	96.55%
SH2	0	24	5	82.76%
SH3	1	5	23	79.31%
PASSIVE	SH1	SH2	SH3	Relative Accuracy
SH1	35	0	1	97.22%
SH2	1	29	6	80.56%
SH3	0	7	29	80.56%

After choosing the model, we analyzed the Bode diagram of the TF shown in Fig. 8, concluding that the system exhibits an expected low pass behavior with a cut frequency at −3 dB at 2.28 Hz and a cut frequency at −6 dB at 3.32 Hz. These results are in agreement with those obtained with the W-FYD [16].

V. EXPERIMENTS AND RESULTS

Considering that the WFYD-AIR used the same fabric and exhibits the same characteristics of W-FYD in terms of stiffness workspace, transfer function, and dynamic response, it is reasonable to assume that it provides a comparable perceptual response. Nonetheless, we performed experiments with 5 participants to prove the effectiveness of WFYD-AIR in conveying reliable softness-related and sliding cues.

In the first experimental phase, hereafter called the Relative Recognition Task, we asked participants to probe and sort for softness three different non-linear force-indentation profiles reproduced by W-FYD AIR. The device was commanded to provide the levels of nonlinear stiffness, by controlling the

TABLE II
SUBJECTIVE QUESTIONNARIE

(a) W-FYD AIR Quantitative Evaluation Questionnaire

	Questions	W-FYD-AIR (Mean±SD)
Q1	It was easy to wear and use the W-FYD AIR device	6.50±0.58
Q2	It was feeling uncomfortable while using the W-FYD AIR	2.00±1.41
Q3	I was well isolated from external noises	6.75±0.50
Q4	I was able to hear the sounds made by the actuators of the W-FYD AIR	3.25±2.50
Q5	The stimuli provided by the cutaneous device were enough to discriminate the softness	6.00±1.15
Q6	The stimuli provided by the cutaneous device were enough to discriminate the direction of sliding	6.75±0.50
Q7	At the end of the experiment I felt tired	1.25±0.50
Q8	It was easy to move my hand and fingers while wearing the cutaneous device	6.00±1.41
Q9	I felt hampered by the W-FYD AIR	1±0.00
Q10	The stimuli provided by the cutaneous device on the fingertip felt strange	1.50±0.57
Q11	I felt the stimuli provided by the cutaneous device only on the fingertip	6.75±0.50

(b) Comfort and Fit Questionnaire for Device Comparison

	Questions	W-FYD-AIR (Mean±SD)	W-FYD (Mean±SD)	p-value
Q1	How comfortable do you find the device while wearing it?	3.88 ± 0.33	2.66 ± 0.70	0.0019
Q2	How heavy does the device feel?	2.22 ± 0.97	3.55 ± 0.52	0.0023
Q3	How much does the device restrict finger movement?	2.33 ± 0.86	0.0004	3.88± 0.60
Q4	How easy is it to put on and take off the device?	4.77 ± 0.44	4.55 ± 0.52	0.6199
Q5	How well does the device stay in place during use?	4.56 ± 0.42	3.33 ± 0.86	0.0023
Q6	How well does the device adapt to the shape of your finger?	4.22 ± 0.67	3.22 ± 0.83	0.0125
Q7	How would you rate the overall sensation of wearing this device?	4.11 ± 0.33	2.77 ± 0.66	0.0004
Q8	Which device do you prefer in terms of overall comfort?	100%	0%	
Q9	Which device feels more suitable for prolonged use?	100%	0%	
Q10	Which device provides a better fit?	100%	0%	

motors to reproduce a power force-indentation profile in both active and passive modes. In the second experimental phase, referred to as Tangential Displacement Discrimination, the performances in discriminating the entity of the sliding stimulus are evaluated. We programmed our device to induce right and left displacement on the user's finger-pad by rotating motors clockwise and counter-clockwise, respectively. Finally, we report the results of a subjective quantitative evaluation by participants about W-FYD wearability and effectiveness in haptic multi-cue delivery based on the Likert-type scale.

A. Participants

Five healthy participants (2 Female, Age mean ± SD: 26.6 ± 1.14) gave their informed consent to participate in the experimental campaign. None had physical limitations that could affect the results. Alongside discrimination tests, participants also completed a subjective quantitative evaluation. An additional 10 participants (2 Females, age 28.25 ± 2.43) were recruited to compare the improvements of the W-FYD AIR with the previous one. We asked them to try both in free exploration tasks and fill out a subjective comfort questionnaire.

B. Experimental Setup

Participants were comfortably seated in front of an office desk on a chair, regulable in height, allowing them to comfortably rest their forearm in a comfortable position. All participants wore the W-FYD AIR on the index finger, keeping the finger-pad in correspondence to the fabric stripe and the fingernail below the IR sensor of the device. An auditory pink noise was delivered to the participants via headphones for the entire experiment to prevent the perception of sounds coming from the device's motors. Additionally, the view of the device has been obscured to users to avoid visual perception. The isolation from visual and acoustic cues guarantees the concentration solely on the tactile stimuli. A custom C-written software managed all conducted experiments.

1) Relative Recognition Task: In the first part of the relative recognition task, we tested the softness ordering capability in active mode by considering three different non-linear softness. Referring to (1), several λ values were considered. Since no differences exist in the active mode between W-FYD [16] and W-FYD AIR - the new device can cover the same stiffness workspace of the previous one -, we selected the power function, $F(\delta) = \lambda\delta^{1.40}$, which best covers the stiffness workspace. Specifically, the same three λ values of [16] were used: the lower bound ($\lambda = 0.09$), the reference value ($\lambda = 0.12$), and the higher bound ($\lambda = 0.15$). We presented to the participants these three values of λ in nine sets, each containing three stimuli rendered in random order. For each set, we asked them to probe and sort the provided stimuli based on perceived softness. In the second part of the task, we tested the passive mode. As the input of the pneumatic actuation controller, we chose a sinusoidal signal $A_m sin(2\pi\omega t)$, where A_m is the pressure amplitude, with a frequency of 3 Hz. The theta command for the DC motors is the same one applied for active mode, with δ defined through the bag pressure read with the pressure sensor and converted in indentation using (3). The same three values of λ were presented in 36 sets, with the three stimuli reproduced in random order for each set. As before, the participants had to sort the three stimuli of each set in terms of softness. In both stages, participants did not have time limitations and could ask for the repetition of the same stimuli sequence. Answers were saved on a file for the consequent analysis. Through a customized Matlab script, results were analyzed by summing the results for all subjects in a confusion matrix and reporting the perceived softness versus the rendered one. In the confusion matrix, each row represents the instances in an actual class, while each column represents the instances in a predicted class.

2) Tangential Displacement Discrimination: In the first part of this experimental stage, we analyze the capability of the W-FYD AIR to return sliding direction feedback. In total, 30 tangential sliding stimuli of 10 mm, 15 to the right, and 15 to the left, at 35 mm/s, were presented in a pseudo-random order to the participants. We presented each stimulus once and asked the subject to answer immediately, giving the sliding direction perceived. In the second part, we concentrated on analyzing the capability to discriminate the stimuli length. To this aim, two stimuli were presented, one short 10 mm and one long 15 mm, and the participant had to report which of the two was felt as larger. After the training phase, 28 stimuli, 14 to the right (short and longer) and 14 to the left (short and longer), were presented in a pseudo-random order to the participants.

C. Experimental Results

Results of the Relative Recognition Task, for both Active and Passive mode, are shown in Table I. We reported the perceived versus artificially reproduced softness and the accuracy of discrimination for each softness value. The average recognition rates are $86.21\% \pm 9.12\%$ (mean $\pm$ SD) and $86.11\% \pm 9.62\%$ (mean $\pm$ SD) for active and passive modes, respectively, which are coherent with the ones obtained with the W-FYD in [16]. These results indicate that the device can render different softness levels well recognizable by the participants in both working modalities. Results of the Tangential Displacement Discrimination are equal to 100% for the absolute left/right discrimination (coherent with those obtained in [16]) and 94.7% (left/right mean) for the left short/long discrimination.

Table II(a) and II(b), present the mean values and standard deviations of participants' responses to the subjective quantitative evaluation and subjective comfort and fit questionnaires, respectively. In Table II(b), a score of 1 indicates "totally disagree" and 7 indicates "totally agree." Results show that participants found the W-FYD AIR wearable and comfortable (Q1, Q2, Q8, Q9), with positive feedback on the perception of softness and sliding sensations (Q5, Q6), which were perceived as natural (Q10). The stimuli, experienced only at the fingertip, further demonstrate the device's wearability (Q11). Participants also rated the experimental conditions favorably (Q3) and found the experimental load manageable (Q7). However, Q4 responses suggest the actuator noise, especially from the inflating system, could be improved. Results in Table II(b), where 1 indicates "not at all" and 5 "completely," highlight that participants preferred the new W-FYD AIR, thanks to its better comfort, wearability, and reduced footprint.

VI. Discussions and Conclusions

In this work, we introduced the miniaturized version of the W-FYD [16], named W-FYD AIR, with dimensions reduced from $100 \times 60 \times 36$ mm to $78 \times 45 \times 37$ mm and weight from 100 g to 54 g. We mainly acted by replacing the servo motor in the lifting mechanism for passive exploration with pneumatic actuation. The lifting mechanism is fundamental for the uniqueness of the device, since it enables to decouple contact force and area growth, allowing passive exploration and tactile AR appllications [15]. Characterization tests confirmed that the W-FYD AIR covers the same stiffness range as the original device in both active and passive modes. The system displayed the expected low-pass behavior, with a -3 dB cut-off frequency of around 3 Hz, consistent with previous findings [16]. To evaluate the device's effectiveness, we conducted experiments with five subjects. Results showed high rate percentages, coherent with those of the original W-FYD, demonstrating the device's ability to render different softness levels and elicit clear sliding perception. Finally, we reported the results of the subjective questionnaires, which highlight that subjects appreciate the comfort and wearability of the device, also w.r.t. the previous version, and, particularly, the natural perception of the rendered tactile stimuli. While the W-FYD AIR is unique in its capability to modulate softness perception in a *Feel-through* way and to allow active and passive interaction modes, in future works it will be interesting to compare it with other solutions. On-going work is devoted to encapsulating the remotized parts in a unique sound-proofed case (to reduce the noise which is an aspect to improve) that can be comfortably worn on the forearm. Preliminary results are encouraging but further works are required. Having a completely wearable solution with an improved form factor can open interesting applications of tAR, e.g., for training in medical applications or industrial settings, as well as in telerobotics. Preliminary tests for robotics-enabled tele-palpation in gynecological surgery are currently ongoing. The reduced dimensions of the system can also enable a multi-digit implementation, which is currently under evaluation.

References

[1] C. Pacchierotti, S. Sinclair, M. Solazzi, A. Frisoli, V. Hayward, and D. Prattichizzo, "Wearable haptic systems for the fingertip and the hand: Taxonomy, review, and perspectives," *IEEE Trans. haptics*, vol. 10, no. 4, pp. 580–600, Oct.–Dec. 2017.

[2] R. Traylor and H. Z. Tan, "Development of a wearable haptic display for situation awareness in altered-gravity environment: Some initial findings," in *Proc. 10th IEEE Symp. Haptic Interfaces Virtual Environ. Teleoperator Syst. HAPTICS 2002*, 2002, pp. 159–164.

[3] S. F. M. Toh, K. N. Fong, P. C. Gonzalez, and Y. M. Tang, "Application of home-based wearable technologies in physical rehabilitation for stroke: A scoping review," *IEEE Trans. Neural Syst. Rehabil. Eng.*, vol. 31, pp. 1614–1623, 2023.

[4] D. Leonardis, M. Solazzi, I. Bortone, and A. Frisoli, "A 3-RSR haptic wearable device for rendering fingertip contact forces," *IEEE Trans. haptics*, vol. 10, no. 3, pp. 305–316, Jul.–Sep. 2017.

[5] M. Bianchi et al., "Design and preliminary affective characterization of a novel fabric-based tactile display," in *Proc. 2014 IEEE Haptics Symp.*, 2014, pp. 591–596.

[6] C. Pacchierotti, F. Chinello, M. Malvezzi, L. Meli, and D. Prattichizzo, "Two finger grasping simulation with cutaneous and kinesthetic force feedback," in *Proc. Haptics: Perception, Devices, Mobility, Commun.*, Tampere, Finland, 2012, pp. 373–382.

[7] D. Doria, S. Fani, A. Giannini, T. Simoncini, and M. Bianchi, "Enhancing the localization of uterine leiomyomas through cutaneous softness rendering for robot-assisted surgical palpation applications," *IEEE Trans. Haptics*, vol. 14, no. 3, pp. 503–512, Jul.–Sep. 2021.

[8] Y. Huang et al., "Recent advances in multi-mode haptic feedback technologies towards wearable interfaces," *Mater. Today Phys.*, vol. 22, 2022, Art. no. 100602.

[9] X. Ji et al., "Untethered feel-through haptics using 18-μm thick dielectric elastomer actuators," *Adv. Funct. Mater.*, vol. 31, no. 39, 2021, Art. no. 2006639.

[10] A. Withana, D. Groeger, and J. Steimle, "Tacttoo: A thin and feel-through tattoo for on-skin tactile output," in *Proc. 31st Annu. ACM Symp. User Interface Softw. Technol.*, 2018, pp. 365–378.

[11] S.-Y. Teng, A. Gupta, and P. Lopes, "Haptic permeability: Adding holes to tactile devices improves dexterity," in *Proc. CHI Conf. Hum. Factors Comput. Syst.*, 2024, pp. 1–12.

[12] S.-Y. Teng, P. Li, R. Nith, J. Fonseca, and P. Lopes, "Touch&Fold: A foldable haptic actuator for rendering touch in mixed reality," in *Proc. 2021 CHI Conf. Hum. Factors Comput. Syst.*, 2021, pp. 1–14.

[13] S. V. Salazar, C. Pacchierotti, X. de Tinguy, A. Maciel, and M. Marchal, "Altering the stiffness, friction, and shape perception of tangible objects in virtual reality using wearable haptics," *IEEE Trans. Haptics*, vol. 13, no. 1, pp. 167–174, Jan.–Mar. 2020.

[14] Y. Tao, S.-Y. Teng, and P. Lopes, "Altering perceived softness of real rigid objects by restricting fingerpad deformation," in *Proc. 34th Annu. ACM Symp. User Interface Softw. Technol.*, 2021, pp. 985–996.

[15] S. Fani, S. Ciotti, G. Pagnanelli, A. Moscatelli, Y. De Pra, and M. Bianchi, "Modulating the perceived softness of real objects through wearable haptics," *IEEE Trans. Haptics*, vol. 16, no. 4, pp. 543–548, Oct.–Dec. 2023.

[16] S. Fani, S. Ciotti, E. Battaglia, A. Moscatelli, and M. Bianchi, "W-FYD: A wearable fabric-based display for haptic multi-cue delivery and tactile augmented reality," *IEEE Trans. Haptics*, vol. 11, no. 2, pp. 304–316, Apr.–Jun. 2018.

[17] A. bicchi, E. Scilingo, and D. De Rossi, "Haptic discrimination of softness in teleoperation: The role of the contact area spread rate," *IEEE Trans. Robot. Automat.*, vol. 16, no. 5, pp. 496–504, Oct. 2000.